CHEMISTRY OF MATERIALS
Article

Chem. Mater. **2010,** *22,* 935–941 935
DOI:10.1021/cm901824c

High-Temperature Transport Properties of the Zintl Phases $Yb_{11}GaSb_9$ and $Yb_{11}InSb_9$†

Tanghong Yi,‡ Catherine A. Cox,‡ Eric S. Toberer,§ G. Jeffrey Snyder,§ and Susan M. Kauzlarich*,‡

‡*Department of Chemistry, University of California, One Shields Avenue, Davis, California 95616, and* §*Materials Science, California Institute of Technology, 1200 California Boulevard, Pasadena, California 91125*

Received June 26, 2009. Revised Manuscript Received October 29, 2009

Two rare-earth Zintl phases, $Yb_{11}GaSb_9$ and $Yb_{11}InSb_9$, were synthesized in high-temperature self-fluxes of molten Ga and In, respectively. Structures were characterized by both single-crystal X-ray diffraction and powder X-ray diffraction and are consistent with the published orthorhombic structure, with the space group *Iba*2. High-temperature differential scanning calorimetry (DSC) and thermal gravimetry (TG) measurements reveal thermal stability to 1300 K. Seebeck coefficient and resistivity measurements to 1000 K are consistent with the hypothesis that $Yb_{11}GaSb_9$ and $Yb_{11}InSb_9$ are small band gap semiconductors or semimetals. Low doping levels lead to bipolar conduction at high temperature, preventing a detailed analysis of the transport properties. Thermal diffusivity measurements yield particularly low lattice thermal conductivity values, less than 0.6 W/m K for both compounds. The low lattice thermal conductivity suggests that $Yb_{11}MSb_9$ (M = Ga, In) has the potential for high thermoelectric efficiency at high temperature if charge-carrier doping can be controlled.

Introduction

Thermoelectric devices directly convert heat flow into electrical power via the Seebeck effect.[1−4] Current applications for thermoelectric devices are limited by the energy conversion efficiency of thermoelectric materials. The dimensionless figure of merit $zT = \alpha^2 T/\rho\kappa$ is used to evaluate the energy conversion efficiency of thermoelectric materials, where α is the Seebeck coefficient, T is the temperature, ρ is the electrical resistivity, and κ is the thermal conductivity. The ideal thermoelectric material possesses both low electrical resistivity and low thermal conductivity, termed "electron crystal and phonon glass" by Slack.[5] Current research on thermoelectric materials is concentrated on: (I) improving existing materials through the use of dopants and nanostructures to alter the electronic and thermal properties[6−8] and (II) the discovery of new materials with superior thermoelectric properties.[2,4]

One of the most promising classes of materials with potential to fulfill the "electron-crystal phonon-glass" physical property requirement are the Zintl phases.[9] Zintl phases are valence-precise semiconductors made up of electropositive cations (typically, group 1 and 2 and more recently broadened to include rare-earth elements) and electronegative anions (typically, group 13−16).[10] The filled skutterudites, clathrates, and $Yb_{14}MnSb_{11}$ all qualify as Zintl compounds with peak zT values of unity or greater when the carrier concentration is appropriately controlled.[11−13] All of these materials have lattice thermal conductivity values of 1 W/m K or less because of their structural complexity. We have been particularly interested in controlling the electronic properties of $Yb_{14}MnSb_{11}$ by alloying on the rare earth and transition metal sites.[12,14,15] Here we discuss the potential for

† Accepted as part of the 2010 "Materials Chemistry of Energy Conversion Special Issue".

*Corresponding author.

(1) Tritt, T. M. *Science* **1996**, *272*, 1276.
(2) Goldsmid, H. J.; Nolas, G. S. *20th International Conference on Thermoelectric*; IEEE: Piscataway, NJ, 2001.
(3) DiSalvo, F. J. *Science* **1999**, *285*(5428), 703–706.
(4) Snyder, G. J.; Toberer, E. S. *Nat. Mater.* **2008**, *7*, 105–114.
(5) *CRC Handbook of Thermoelectrics*; Rowe, D. M., Ed.; CRC Press: Boca Raton, FL, 1995; p 410.
(6) Heremans, J. P.; Jovovic, V.; Toberer, E. S.; Saramat, A.; Kurosaki, K.; Charoenphakdee, A.; Yamanaka, S.; Snyder, G. J. *Science* **2008**, *321*, 554–557.
(7) Venkatasubramanian, R.; Siivola, E.; Colpitts, T.; O'Quinn, B. *Nature* **2001**, *413*, 597–602.
(8) Hicks, L. D.; Dresselhaus, M. S. In *Growth, Processing, and Characterization of Semiconductor Heterostructures Symposium*; Mater. Res. Soc: Boston, MA, 1994; pp 413−418.
(9) Kauzlarich, S. M.; Brown, S. R.; Snyder, G. J. *Dalton Transactions* **2007**, 2009.
(10) Nesper, R. *Prog. Solid State Chem.* **1990**, *20*(1), 1–45.
(11) Nolas, G. S.; Poon, J.; Kanatzidis, M. G. *MRS Bull.* **2006**, *31*(3), 199–205.
(12) Brown, S. R.; Kauzlarich, S. M.; Gascoin, F.; Snyder, G. J. *Chem. Mater.* **2006**, *18*, 1873–1877.
(13) Saramat, A.; Svensson, G.; Palmqvist, A. E. C.; Stiewe, C.; Mueller, E.; Platzek, D.; Williams, S. G. K.; Rowe, D. M.; Bryan, J. D.; Stucky, G. D. *J. Appl. Phys.* **2006**, *99*, 023708.
(14) Toberer, E. S.; Cox, C. A.; Brown, S. R.; Ikeda, T.; May, A. F.; Kauzlarich, S. M. *Adv. Funct. Mater.* **2008**, *18*, 2795–2800.
(15) Brown, S. R.; Toberer, E. S.; Ikeda, T.; Cox, C. A.; Gascoin, F.; Kauzlarich, S. M.; Snyder, G. J. *Chem. Mater.* **2008**, *20*, 3412–3419.

© 2009 American Chemical Society
Published on Web 11/23/2009

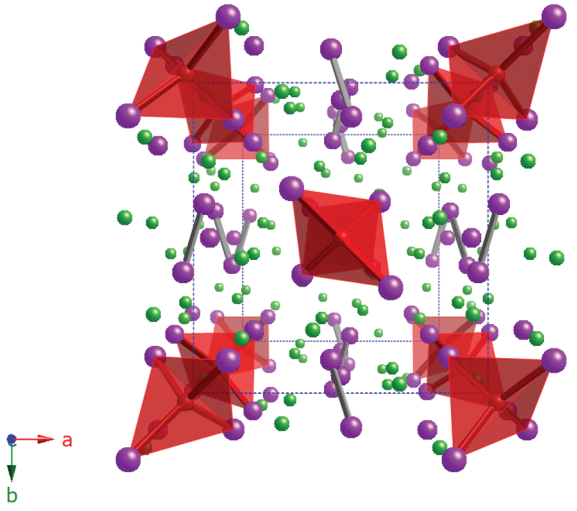

Figure 1. Crystal structure of $Yb_{11}MSb_9$ (M = Ga, In) viewed down the c-axis (unit cell is outlined). The MSb_4^{9-} tetrahedra are highlighted red polyhedra with red In atoms in the centers. Isolated Sb^{3-} anions are purple and Sb_2^{4-} dimers are connected by bonds; Yb^{2+} cations are in green.

thermoelectric applications in the structurally related $Yb_{11}MSb_9$ (M = Ga, In) compounds.

The compounds $Yb_{11}MSb_9$ (M = Ga, In), with the $Ca_{11}InSb_9$-type structure,[16,17] were first reported by Bobev et al. ($Yb_{11}GaSb_9$) in 2005 and Xia et al. ($Yb_{11}InSb_9$) in 2007.[18,19] The structure of $Yb_{11}MSb_9$ (M = Ga, In) is closely related to $Ca_{14}AlSb_{11}$ structure type.[20] $Yb_{14}MnSb_{11}$, which is isostructural to $Ca_{14}AlSb_{11}$,[20] can be described as 14 Yb^{2+} cations, one $[MnSb_4]^{9-}$ tetrahedral, a $[Sb_3]^{7-}$ linear trimer and 4 isolated Sb^{3-} anions.[12] The structure of $Yb_{11}MSb_9$, shown in Figure 1, can be viewed as containing 11 Yb^{2+} cations, one $[MSb_4]^{9-}$ tetrahedron, one $[Sb_2]^{4-}$ dimer and 3 isolated Sb^{3-} anions based on the Zintl formalism and rules for electron counting. The tetrahedra and dimers are packed in an eclipsed and alternating fashion in both the a and b directions.

Prior measurements of the electrical resistivity of $Yb_{11}GaSb_9$ reveal decreasing resistivity with increasing temperature below 250 K, associated with carrier activation.[18] Above this temperature, phonon-dominated mobility leads to an increasing resistivity with temperature. Electronic structure calculations of $Yb_{11}GaSb_9$ suggest a small band gap (~0.03 eV).[18] In contrast, prior measurements of $Yb_{11}InSb_9$ reveal metallic behavior with decreasing resistivity with decreasing temperature.[19] Xia et al. suggest these differences arise from differences in band gap size—$Yb_{11}GaSb_9$ is likely a small band gap semiconductor, whereas $Yb_{11}InSb_9$ is likely a semimetal.[19] A similar decrease in band gap is observed in the analogous $Ca_{11}MSb_9$ (M = Ga, In).[17] This paper presents the high temperature stability and thermoelectric properties of $Yb_{11}MSb_9$ (M = Ga, In).

Experimental section

Synthesis. All materials were handled in a nitrogen filled glovebox or with other inert atmosphere techniques. Sublimed dendritic ytterbium metal (Stanford Materials Corporation, 99.99%) was cut into small pieces. Sb shot (Alfa Aesar, 99.9%), Ga pellets (Alfa Aesar, 99.9999%) and In drops (CERAC, 99.99%) were used as received. The starting materials were loaded in a 5 mL alumina crucible with stoichiometric ratio of Yb:M:Sb (M = Ga, In) at 11:76:9. The crucible was put in a fused silica ampule with quartz wool on the top and at the bottom, which was then sealed under a vacuum.

The reaction was heated in a programmable furnace (Barnstead Thermolyne 4800) under the following temperature profile: heating to 773 K from room temperature in 2 h, and dwell at 773 K for 6 h, then ramping to 1273 K within 2 h and dwell 6 h at 1273 K, followed by cooling to 873 K at a rate of 2 K/h. At this point, the ampule was quickly removed from the furnace, inverted and centrifuged to remove the extra flux. Details on the flux-growth synthesis procedures have been discussed elsewhere.[19,21] The ampule was opened in a nitrogen-filled glovebox in order to obtain the crystals.

The crystals of $Yb_{11}GaSb_9$ and $Yb_{11}InSb_9$ show surface oxidation after a few hours exposure in air. However, no significant change can be observed in powder X-ray diffraction after exposed in air for several days. The crystals of $Yb_{11}MSb_9$ (M = Ga, In) do not decompose in air or water, but $Yb_{11}GaSb_9$ was reported to dissolve in mineral acids.[18]

Single-Crystal and Powder X-ray Diffraction. In a nitrogen-filled glovebox, single crystals of $Yb_{11}MSb_9$ (M = Ga, In) were placed in a vial filled with paratone oil in order to prevent oxidation during transport. A properly sized crystal was selected and positioned at the tip of a glass fiber. The fiber with the crystal attached was quickly moved to a nitrogen steam for single-crystal diffraction. Diffraction data were acquired using a Bruker SMART 1000 CCD diffractometer utilizing a graphite-monochromatic Mo Kα radiation (λ = 0.71069 Å) at 90 (2) K with operating voltage and current of 50 kV and 30 mA, respectively. The SMART software was employed for data acquisition, and SAINT was used for spot integrations. Multi-scan absorption corrections for Lorentz and polarization effects were performed with SADABS program. XPREP was used to identify the space group and to create the data files. The structure solution was obtained by direct methods and refined with the SHELXTL 5.10 package.[22]

Several crystals were ground into a powder and loaded into an air sensitive holder for X-ray powder diffraction (XRD). XRD data were collected by a Bruker D8 diffractometer with Cu Kα radiation (λ = 1.54060 Å) to analyze purity. Data acquisition was performed with Bruker software, analysis and refinement for lattice parameters was performed using MDI JADE 6.1. The whole pattern fit refinements were performed with X'Pert HighScore program.[23]

Microprobe Measurement. Microprobe measurements were obtained on single crystals using a Camera SX-100 Electron

(16) Cordier, G.; Schafer, H.; Stelter, M. *Z. Naturforsch., Sect. B* **1985**, *40*(7), 868–871.
(17) Young, D. M.; Kauzlarich, S. M. *Chem. Mater.* **1995**, *7*(1), 206–209.
(18) Bobev, S.; Fritsch, V.; Thompson, J. D.; Sarrao, J. L.; Eck, B.; Dronskowski, R.; Kauzlarich, S. M. *J. Solid State Chem.* **2005**, *178*, 1071–1079.
(19) Xia, S.-q.; Hullmann, J.; Bobev, S.; Ozbay, A.; Nowak, E. R.; Fritsch, V. *J. Solid State Chem.* **2007**, *180*, 2088–2094.
(20) Cordier, G.; Schafer, H.; Stelter, M. *Z. Anorg. Allg. Chem* **1984**, *519*, 183.
(21) Canfield, P. C.; Fisk, Z. *Philos. Mag., B* **1992**, *65*(6), 1117–1123.
(22) Sheldrick, G. M., Acta Crystallogr., Sect. A **2008**, *64* (112−122), 112.
(23) *X'Pert HighScore*; PANalytical B.V.: Almelo, the Netherlands, 2004.

Probe Microanalyzer equipped with a wavelength-dispersive spectrometer. The samples were prepared by mounting crystals encased in epoxy and coated with carbon onto 25 mm metal rounds by means of adhesive carbon tapes. The surfaces of samples were polished to ensure the smooth surfaces and to remove surface oxidation. Pure elements, Yb and Sb, and the compounds, InAs and GaAs, were used as calibration standards. Each sample was scanned with a spot size of 1 μm and data collected at 14 points along its surface. The compositions were calculated as the average of the 14 points.

Thermogravimetry and Differential Scanning Calorimetry (TG/DSC). Data were collected by a Netzsch Thermal Analysis STA 409 cell equipped with a TASC 414/2 controller and PU 1.851.01 power unit. After the baselines were established, a pellet made from ground powder of single crystals was placed into an alumina crucible and run between room temperature and 1473 K under an argon flow at 10 K/min with a data acquisition rate of 10 points/K. Data were acquired using the software provided with the equipment and analyzed with Netzsch Proteus computer program.

Thermoelectric Property Sample Preparation. Finely ground polycrystalline powder from single crystals was hot-pressed in high-density graphite dies in order to achieve dense samples. Cylinder shaped samples were obtained after hot-pressing that were 12 mm diameter and approximately 6.5 mm long. Hot-pressing was conducted at 140 MPa and 1073 K for 2 h under an argon atmosphere. Samples for electric and thermal transport properties and Seebeck coefficient measurements were cut from the cylinder with diamond saw into disks (typically 1 mm thick).

Resistivity Measurement and Hall Effect. The electrical resistivity (ρ) was measured using the van der Pauw technique with a special high temperature apparatus[24] and a current of 100 mA. The Hall coefficient was also measured in the same apparatus with a constant magnetic field about 10000 Gauss. The carrier density (n) was calculated from the Hall coefficient (R_H) based on $n = 1/R_H e$ assuming a scattering factor of 1.0 in a single carrier scheme, where n is carrier density, R_H is the Hall coefficient, and e is the charge of the electron. The Hall mobility (μ_H) was calculated from the Hall coefficient (R_H) and the resistivity values according to equation $\mu_H = R_H/\rho$.

Thermal Conductivity Measurement. The thermal diffusivity was measured using a flash diffusivity technique (LFA475, NETSZCH) with a PyroCeram 9606 standard. The thermal conductivity was calculated according to the equation $\kappa = C_p dD$, where the heat capacity (C_p) was estimated using the Dulong–Petit value of C_v, geometric density (d), and thermal diffusivity (D) from experimental data.

Seebeck Coefficient Measurement. The Seebeck coefficient was measured using a high-temperature light pulse technique with chromel/Nb thermocouples. A small auxiliary heater was employed to produce a temperature difference ΔT between both ends of the sample. The thermoelectric voltage ΔV and the temperature difference ΔT were measured by a multimeter. Thus, the Seebeck coefficient was calculated by the slope of the line of ΔV vs ΔT.

Results and Discussion

Structure and Phase Characterization. The structures of $Yb_{11}MSb_9$ (M = Ga, In) were determined by single crystal X-ray diffraction. Samples synthesized by the flux method have similar lattice parameters as previously reported.[18,19] The space group is *Iba*2 (No. 45), and the parameters for $Yb_{11}GaSb_9$ and $Yb_{11}InSb_9$ are a = 11.7320(13) Å, b = 12.3199(13) Å, c = 16.6401(18) Å (R_1 = 3.38%), and a = 11.7891(24) Å, b = 12.4228(25) Å, c = 16.6735(33) Å (R_1 = 4.75%), respectively. The details of the structure of $Yb_{11}MSb_9$ (M = Ga, In), such as coordinates, bonds, distances, and angles, have been discussed by previous researchers.[18,19] Detailed information concerning the structure is not provided in this report as our structure refinement is in good agreement with the previous structural refinements. Figure 1 shows a view of the structure. In brief, the structure consists of MSb_9^{4-} tetrahedra that are at the corners and center of the *ab* plane and periodically repeat every $c/2$ along the c axis. Each Sb_2^{4-} dimer resides between two tetrahedra along a and b axis. X-ray powder diffraction patterns for $Yb_{11}MSb_9$ (M = Ga, In) were used to determine the purity of the phase. The refined patterns provided a good fit to the data with R_p = 5.145%, R_p = 4.294% for $Yb_{11}GaSb_9$ and $Yb_{11}InSb_9$, respectively (Figure 2).[23] The profile refinements of the diffraction patterns indicated 1 wt % Yb_2O_3 and 1 wt % GaSb as contaminants in $Yb_{11}GaSb_9$, and 5 wt % of residual flux In and 1 wt % of Yb_2O_3 in $Yb_{11}InSb_9$.[23] The diffraction peak attributed to In metal in $Yb_{11}InSb_9$ is marked with an asterisk. However, the diffraction peaks attributed to Ga are not discernible in the XRD pattern of $Yb_{11}GaSb_9$, because Ga is expected to

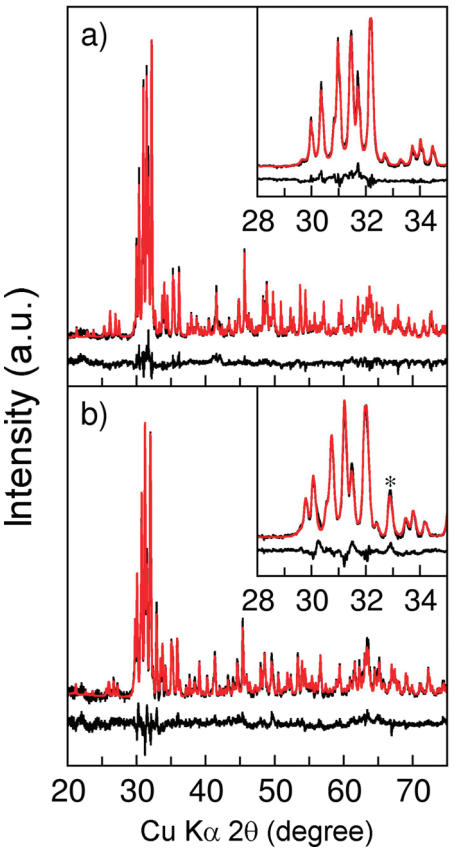

Figure 2. X-ray powder diffraction patterns in black and refined patterns with X'Pert HighScore Plus in red color, and the difference between experimental and refined patterns shown in black; (a) $Yb_{11}GaSb_9$, (b) $Yb_{11}InSb_9$. The insets show an enlarged segment and in (b) a peak assigned to In is marked with asterisk.

(24) McCormack, J. A.; Fleurial, J. P. *Mater. Res. Soc. Symp. Proc.* **1991**, *234*, 135.

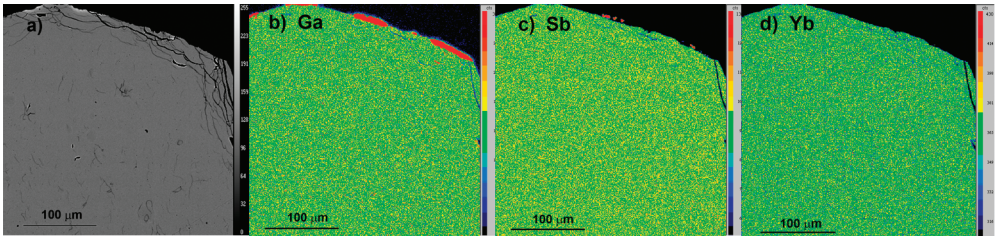

Figure 3. Electron microprobe images of a representative area of a $Yb_{11}GaSb_9$ single crystal. (a) Back scattered electron (BSE) and element mapping images of (b) Ga, (c) Sb, (d) Yb. The relative intensities increase from black (bottom) to red/white (top).

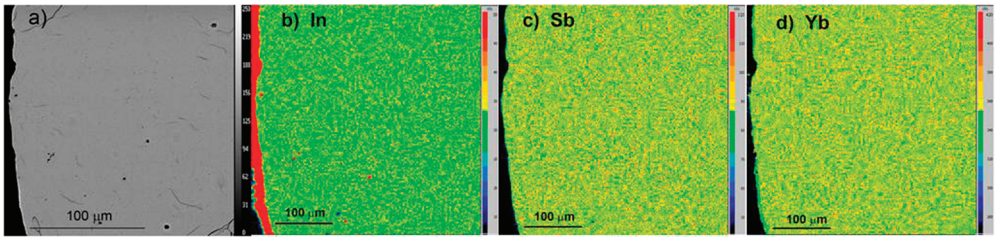

Figure 4. Electron microprobe image of a representative area of a $Yb_{11}InSb_9$ single crystal. (a) Back-scattered electron (BSE) and element mapping images of (b) In, (c) Sb, (d) Yb. The relative intensities increase from black (bottom) to red/white (top).

be amorphous. The presence of In and Ga is a result of incomplete flux removal. Slow surface oxidation leading to Yb_2O_3 was reported by S. Bobev et al.[18]

The microprobe images of backscattered electron (BSE) micrographs and element maps for $Yb_{11}MSb_9$ (M = Ga, In) are shown in Figures 3 and 4. These images are consistent with a homogeneous phase for the crystals presented. The compositions $Yb_{10.96(3)}Ga_{1.00(1)}Sb_{9.17(3)}$ and $Yb_{10.68(2)}In_{1.00(1)}Sb_{9.00(2)}$ represent the average distribution of the major phase for each compound. The Yb content for $Yb_{11}GaSb_9$ is slightly low, which might be a result of a surface oxidation of the crystals. The Yb content for $Yb_{11}InSb_9$ is less than ideal, however, no non-stoichiometry was apparent. Microprobe analysis found elemental Ga and In in the grain boundaries of the hot-pressed polycrystalline samples (Supporting Information).

Thermal Stability. $Yb_{11}MSb_9$ (M = Ga, In) compounds are thermally stable up to 1334 K (Ga) and 1367 K (In) based on the TG-DSC curves in Figure 5. No significant mass change was observed according to the TG curves. The continual minor increases in the DSC data observed in both samples as a function of temperature with no weight change are consistent with sintering of the powder during the heating process. The small endothermic peak around 430 K of the DSC curve for $Yb_{11}InSb_9$ is attributed to the melting of residual indium flux (see the enlarged region shown as an inset in Figure 5a). The amount of In flux remaining in the sample can be calculated on the basis of the heat absorbed and is approximately 3.6% by weight. This is consistent with the amount obtained from the XRD refinement. Any residual Ga flux was not detectable because the starting temperature was above the melting point of Ga. The melting endothermic and recrystallization exothermic peaks of the majority phase are shown in the heating and cooling DSC curves. An additional recrystallization

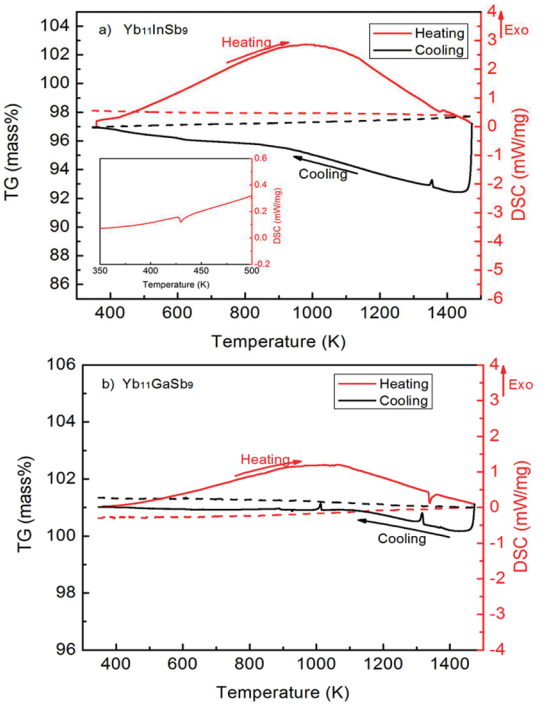

Figure 5. TG (dash lines) and DSC (solid lines) curves for (a) $Yb_{11}InSb_9$ and (b) $Yb_{11}GaSb_9$ obtained under an argon flow at 10 K/min. The melting peak for residual In flux around 430K is shown in the inset of (a). Legend indicates heating and cooling DSC curves. Exothermic heat transfer is positive. Red curves are for heating and black curves are for cooling process.

peak at around 1010 K in the DSC cooling curve for $Yb_{11}GaSb_9$ is attributed to the presence of GaSb binary phase (Figure 5b), which was identified by XRD. The lack of the corresponding melting endotherm is attributed to the relatively high heating rate and poor contact of the GaSb with the crucible. This excellent thermal stability would be an additional benefit to these materials if the thermoelectric properties of $Yb_{11}MSb_9$ can be sufficiently improved (discussed below).

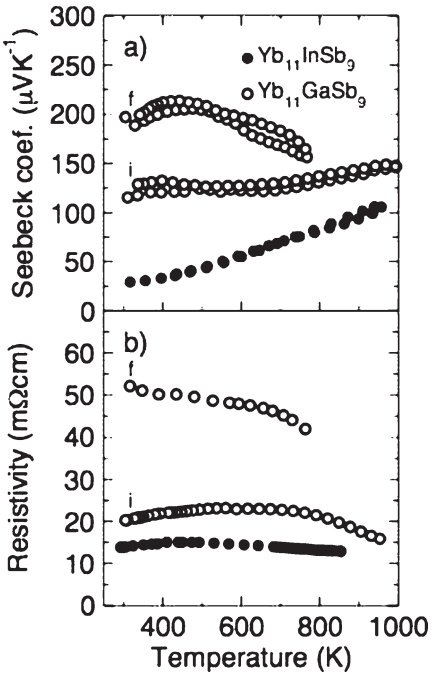

Figure 6. (a) Seebeck coefficient and (b) resistivity measurements of $Yb_{11}MSb_9$, M = Ga, In. Gradual variations in resistivity and Seebeck were observed for subsequent $Yb_{11}GaSb_9$ measurements attributed to changes in carrier concentration (see Figure 7); shown here are the initial (i) and final (f) measurements.

Transport Properties. Prior investigation on the low temperature (1.8 − 400 K) transport of $Yb_{11}GaSb_9$ flux-grown single crystals found decreasing resistivity with increasing temperature, indicative of thermally activated conductivity.[18] From 200 K upward, the resistivity increased, leading to room temperature resistivity values of 30−45 mΩ cm. Polycrystalline slices of $Yb_{11}GaSb_9$ studied here display similar room temperature resistivity values as the samples from the previous study (Figure 6b, 20−50 mΩ cm at 300 K). Hall effect measurements analyzed with a single carrier model $\langle 1/n_H e = R_H \rangle$ (Figure 7) show an exponential increase in carrier concentration and a rapid decrease in mobility with increasing temperature. At higher temperatures (∼700 K), the resistivity begins to decrease as the carrier concentration rise exceeds the rate of mobility decay. Such a rapid rise in carrier concentration is indicative of the thermal excitation of carriers across a small band gap but could also be due to transport across grain boundaries. As both electrons and holes (and grain boundaries) are influencing transport, the single band approximation leads to an over- and underestimation of n_H and μ_H, respectively (eq 1).

$$R_H = \frac{-n\mu_n^2 + p\mu_p^2}{e(n\mu_n + p\mu_p)^2} \quad (1)$$

The Seebeck coefficient of $Yb_{11}GaSb_9$ is large and positive for all temperatures studied. Likewise, the Seebeck coefficient of the high zT $Yb_{14}MnSb_{11}$ ranges from ∼60 μV/K at room temperature to a maximum of 185 μV/K at 1275 K,[12] whereas that of $Yb_{11}Sb_{10}$ is less than 25 μV/K in range of

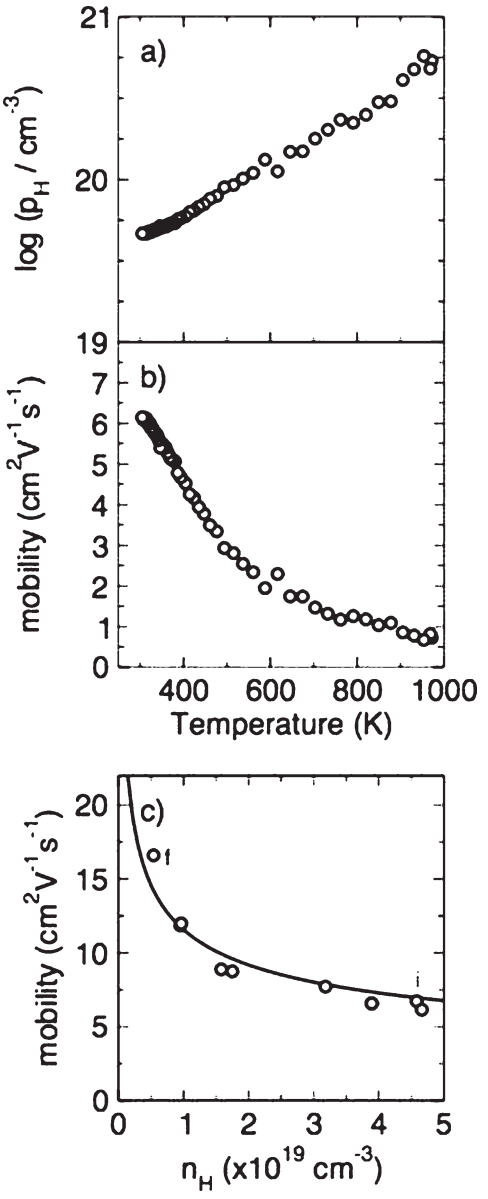

Figure 7. (a) $Yb_{11}GaSb_9$ Hall carrier concentration increases exponentially with temperature (initial measurement shown). (b) The mobility of $Yb_{11}GaSb_9$ decreases with increasing temperature due to increased phonon scattering and increasing carrier concentration (initial measurement shown). (c) Due to the change in $Yb_{11}GaSb_9$ Hall carrier concentration between measurements, room temperature Hall mobility values at a range of carrier concentration were obtained. A $n^{-1/3}$ dependence is observed, consistent with hole transport limited by acoustic phonon scattering.

room temperature to 1000 K.[25] The p-type Seebeck and Hall effect suggests an extrinsic concentration of holes at the ∼10^{19} cm^{-3} level. This is typical with other Zintl compounds (e.g., $Yb_{14}AlSb_{11}$, $Yb_{11}Sb_{10}$, $YbZn_2Sb_2$, and $Yb_5In_2Sb_6$) and is usually attributed to impurities/vacancies.[14,26−28] The nonlinear Seebeck coefficient with

(25) Brown, S. R.; Kauzarich, S. M.; Gascoin, F.; Snyder, G. J. *J. Solid State Chem.* **2007**, *180*(4), 1414–1420.
(26) Gascoin, F.; Ottensmann, S.; Stark, D.; Haile, S. M.; Snyder, G. J. *Adv. Funct. Mater.* **2005**, *15*(11), 1860–1864.
(27) Kim, S. J.; Ireland, J. R.; Kannewurf, C. R.; Kanatzidis, M. G. *J. Solid State Chem.* **2000**, *155*(1), 55–61.
(28) Rauscher, J. F.; Kauzlarich, S. M.; Ikeda, T.; Snyder, G. J. *Z. Anorg. Allg. Chem.* **2007**, *633*(10), 1587–1594.

increasing temperature is reminiscent of $Yb_{14}AlSb_{11}$ and $Yb_{11}Sb_{10}$ where the presence of both n and p carriers led to compensated Seebeck coefficients.[14,25,28,29] Unfortunately, extracting further information from a compensated Seebeck coefficient requires knowledge or assumptions regarding the individual contribution of all bands and grain boundary phases.

Prior measurements of the electrical resistivity of single-crystalline $Yb_{11}InSb_9$ obtained a room temperature resistance of 4 mΩ cm and a linear decrease in resistivity with decreasing temperature (0.006 mΩ cm K^{-1}).[19] Figure 6b shows the room-temperature resistivity of polycrystalline $Yb_{11}InSb_9$ is larger in magnitude but increases linearly to 430 K with a similar slope (0.008 mΩ cm K^{-1}). The large residual resistance term (~11 mΩ cm, extrapolated) may be due to secondary phases between the grains. Above 440 K, the resistivity reversibly decreases with increasing temperature, coinciding with the melting point of In metal. Although liquid indium has a higher resistivity than solid indium, the decreasing resistivity indicates a reduction in the grain boundary resistance and supports the residual resistance assertion. Hall measurements were conducted on $Yb_{11}InSb_9$, but the voltage obtained was below the resolution of the measurement.

The $Yb_{11}InSb_9$ Seebeck coefficient, shown in Figure 6a, is quite small at room temperature (25 μV K^{-1}), and rises linearly with increases temperature through 1000 K. The linear rise and large magnitude of the Seebeck coefficient at high-temperature indicate flux-grown $Yb_{11}InGa_9$ could be a degenerate semiconductor. However, for a semiconductor to remain degenerate at such a high temperature, the band gap and doping levels must be quite large. Alternatively, the unusual behavior (linear rising Seebeck, slightly decreasing resistivity) may be due to grain boundary effects or multiple and/or nonparabolic bands influencing the transport properties. Prior ab inito calculations have suggested f-state bands are near the valence band edge in $Yb_{11}GaSb_9$, which may lead to such nonparabolic band features.[18] Such f-state bands are an optimal situation for high hole effective mass and could be used for high thermoelectric efficiency when tuned appropriately.[30]

Measuring $Yb_{11}MSb_9$ samples to high temperature (> 800 K) was found to cause irreversible changes in the resistivity and Seebeck coefficient. These changes may be attributed to variation in the vacancy/impurity levels and thus variation in the carrier concentration but could also be influenced by changes in the grain boundaries. An unexpected benefit from this variation is the ability to demonstrate the mobility is dominated by acoustic phonon scattering, as seen in the $n_H^{-1/3}$ dependence (fit curve) from a single pellet of $Yb_{11}GaSb_9$ (Figure 7c).[31]

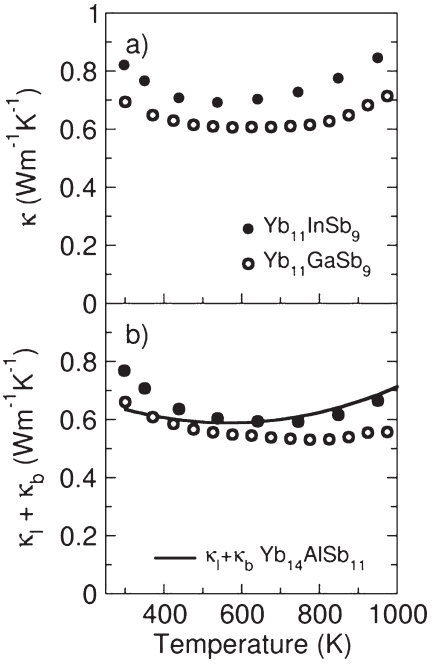

Figure 8. (a) Total thermal conductivity of the title compounds and (b) the lattice and bipolar thermal conductivity obtained by subtracting the electronic component of the thermal conductivity. Similarly low lattice thermal conductivities are found for the Zintl semiconductor $Yb_{14}AlSb_{11}$ shown as a solid line for comparison.[29].

The variation in n_H from 0.5 to 5 × 10^{19} cm^{-3} indicates that broad tunability of carrier concentration can be thus expected from the intentional use of extrinsic dopants.

Thermal conductivity values were calculated ($\kappa = dC_pD$) from the measured density d, the Dulong−Petit approximation of specific heat capacity (C_p), and thermal diffusivity values obtained from flash diffusivity measurements (D). The measured densities of $Yb_{11}InSb_9$ and $Yb_{11}GaSb_9$ are approximately 95 and 96% of the theoretical densities, respectively. Figure 8 shows the temperature dependence of the thermal conductivity for the title compounds and the lattice and bipolar thermal conductivity ($\kappa_L + \kappa_b$) obtained from the subtraction of the electronic thermal conductivity ($\kappa = \kappa_e + \kappa_L + \kappa_b$; $\kappa_e = L\sigma T$; $L = 2.44 \times 10^{-8}$ J^2 K^{-2} C^{-2}). The $\kappa_L + \kappa_b$ values of $Yb_{11}MSb_9$ are low for crystalline materials (less than 0.6 W/mK). Figure 8b also shows the $\kappa_L + \kappa_b$ curve for the structurally similar intrinsic semiconductor $Yb_{14}AlSb_{11}$.[29] In all three of these compounds, heavy atoms in large, complex unit cells lead to extremely low κ_L. Such low thermal conductivities partially contribute to the high zT in doped $Yb_{14}AlSb_{11}$ and may likewise prove to be advantageous in $Yb_{11}MSb_9$. Mixed carriers in all of the materials shown in Figure 8b lead to significant bipolar terms at high temperature.

The figure of merit of unintentionally doped $Yb_{11}MSb_9$ is low, with zT values of ~0.2 and 0.1 at 1000 K for the M = Ga and In compounds, respectively. The low zT values can be a product of mixed carriers and grain boundary effects lowering the Seebeck coefficient and high resistivity values due to a lack of extrinsic dopants. If appropriate dopants can be found and the band gap magnitudes are sufficiently large to prevent bipolar

(29) Cox, C. A.; Toberer, E. S.; Levchenko, A. A.; Brown, S. R.; Snyder, G. J.; Navrotsky, A.; Kauzlarich, S. M. *Chem. Mater.* **2009**, *21*(7), 1354–1360.
(30) Mahan, G. D.; Sofo, J. O. *Proc. Natl. Acad. Sci. U.S.A.* **1996**, *93*(15), 7436–7439.
(31) Toberer, E. S.; Brown, S. R.; Ikeda, T.; Kauzlarich, S. M.; Snyder, G. J. *Appl. Phys. Lett.* **2008**, *93*, 062110.

conduction, good thermoelectric performance may be obtained. We have previously optimized the Zintl semiconductor $Yb_{14}AlSb_{11}$ ($E_g \approx 0.5$ eV) for thermoelectric applications and found extrinsic doping (of Mn^{2+} on the Al^{3+} tetrahedral site) to a carrier concentration of $4-6 \times 10^{20}$ h^+/cm^{-3} increased the peak zT from 0.05 to greater than 1.0.[14]

Conclusions

$Yb_{11}MSb_9$ (M = Ga, In) Zintl phases were successfully synthesized by a self-flux method. Single crystal refinements are consistent with previous reports, and experimental X-ray powder diffraction patterns match the simulated patterns. No phase transitions occur for $Yb_{11}MSb_9$ compounds up to 1300 K according to DSC results. High-temperature polycrystalline resistivity measurements are consistent with prior low-temperature single-crystal results. Flux-grown $Yb_{11}GaSb_9$ may be a small band gap semiconductor, whereas $Yb_{11}InSb_9$ appears to be a degenerate semiconductor or semimetal. In both compounds, the Seebeck coefficient is large and positive at high temperatures, but further analysis is limited by multiband and grain boundary effects. Consistent with the structural relative $Yb_{14}MSb_{11}$, the lattice thermal conductivity of $Yb_{11}MSb_9$ is found to be extremely low (~0.6 W/m K). The figure of merit of $Yb_{11}MSb_9$ is low, approximate 0.2 and 0.1 at 1000 K for M = Ga and In, respectively. Improvements in the thermoelectric performance of $Yb_{11}MSb_9$ may be achieved by optimizing the carrier concentration through extrinsic doping.

Acknowledgment. We gratefully acknowledge the financial support from NSF DMR0600742, the NASA Jet Propulsion Laboratory, and the Beckman Foundation.

Supporting Information Available: A pdf showing the microprobe image and elemental mapping of the hot pressed pellets is provided. This material is available free of charge via the Internet at http://pubs.acs.org.